1974

Advanced Magnetic Methods of Flaw Detection

John R. Barton
Southwest Research Institute

Advanced Magnetic Methods of Flaw Detection

Abstract
Certainly, the area of magnetic testing is old, and what I have to discuss today is a refinement of what has existed for a long time, namely, magnetic field measurement. However, as opposed to the common use of magnetic particles to visually produce a signature, in the magnetic perturbation method the magnetic field is controlled and the specimen is scanned to measure the magnitude and direction of the magnetic field.

Disciplines
Materials Science and Engineering | Structures and Materials

ADVANCED MAGNETIC METHODS OF FLAW DETECTION

John R. Barton
Southwest Research Institute
San Antonio, Texas

Certainly, the area of magnetic testing is old, and what I have to discuss today is a refinement of what has existed for a long time, namely, magnetic field measurement. However, as opposed to the common use of magnetic particles to visually produce a signature, in the magnetic perturbation method the magnetic field is controlled and the specimen is scanned to measure the magnitude and direction of the magnetic field.

In Fig. 1a we see schematically a ferromagnetic specimen with a nonferromagnetic inclusion embedded in the matrix. The relatively uniform magnetic flux is disturbed by the inclusion and, in turn, a leakage flux is produced at the surface. Since the field disturbance is very small, it may be called a perturbation at the surface, and if we scan the region with an electrical conductor at a uniform velocity, we can produce a signature of this general shape, Fig. 1b.

For much of the work that we have done on an Air Force Office of Scientific Research contract, fairly elegant specimens of AISI 4340 steel have been used, Fig. 2. At the time we got our billets for specimen fabrication, aircraft quality was specified. Nonetheless, they had quite a number of inclusions in them, and this was important, since we wanted to study the role of inclusions in nucleating fatigue cracks. We have investigated only a few specimens, but we look to each specimen very intensely. Figure 3 is a view of the experimental apparatus, and the test specimen has been indicated by a circle. A better view of the specimen is presented in Fig. 4 and, in this case, a Hall Effect probe is used to examine about 3/4 inch of the central region or gauge section. The probe can be rotated around the specimen to scan adjacent tracks.

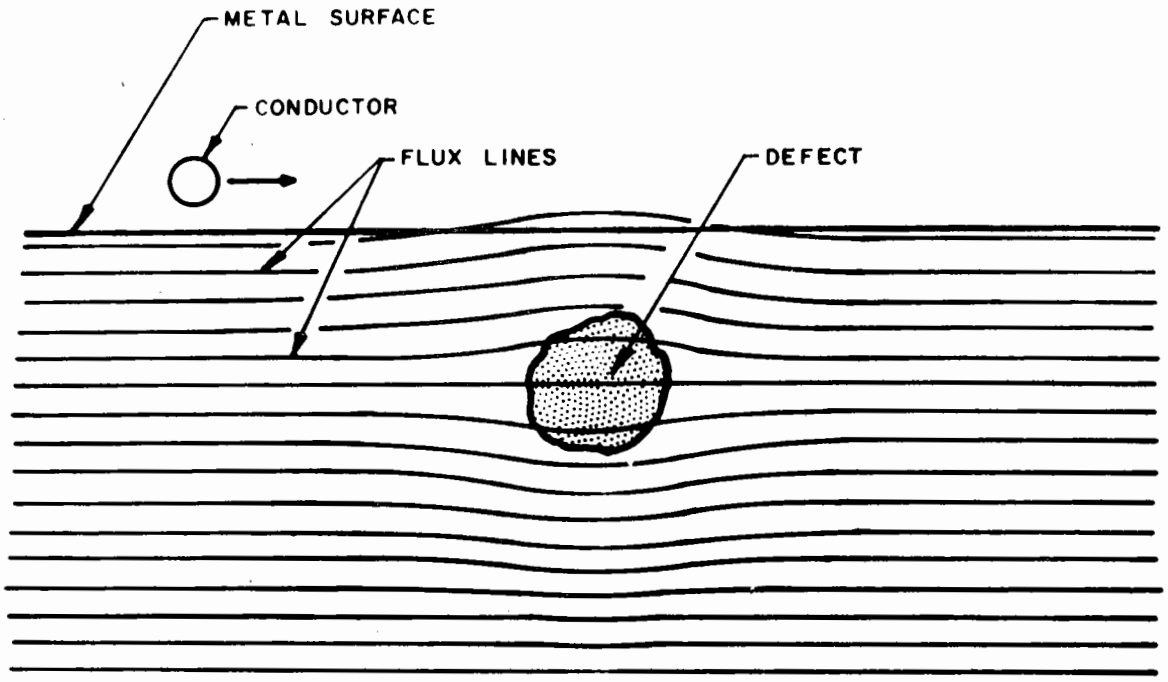

(A) FLUX PERTURBATION

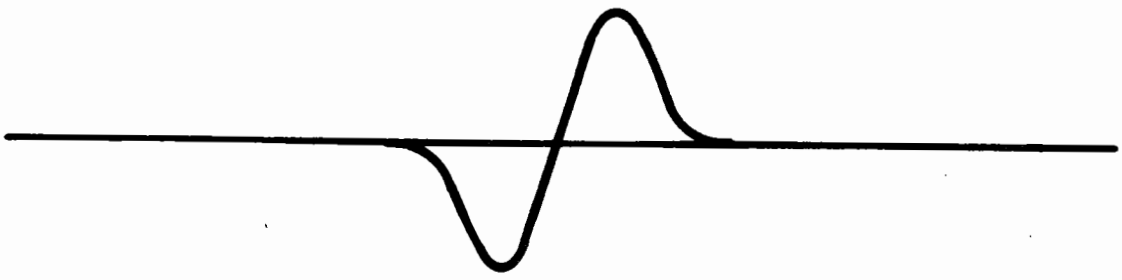

(B) SIGNAL SHAPE AS A FUNCTION OF CONDUCTOR LOCATION

Fig. 1. Perturbations in magnetic flux caused by defect in magnetic material and shape of signal induced in moving conductor.

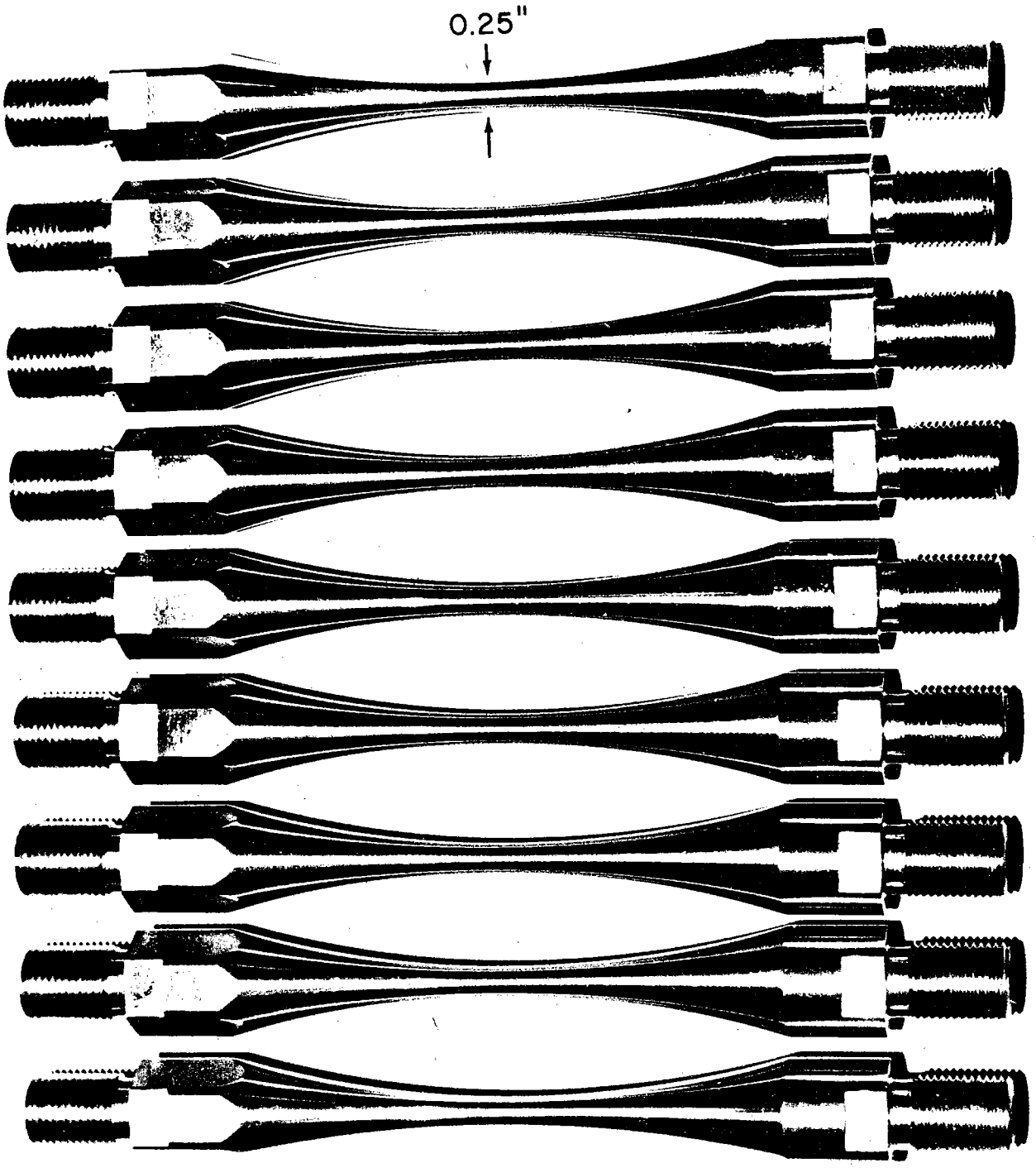

Fig. 2. Photograph showing several typical AISI 4340 steel test specimens.

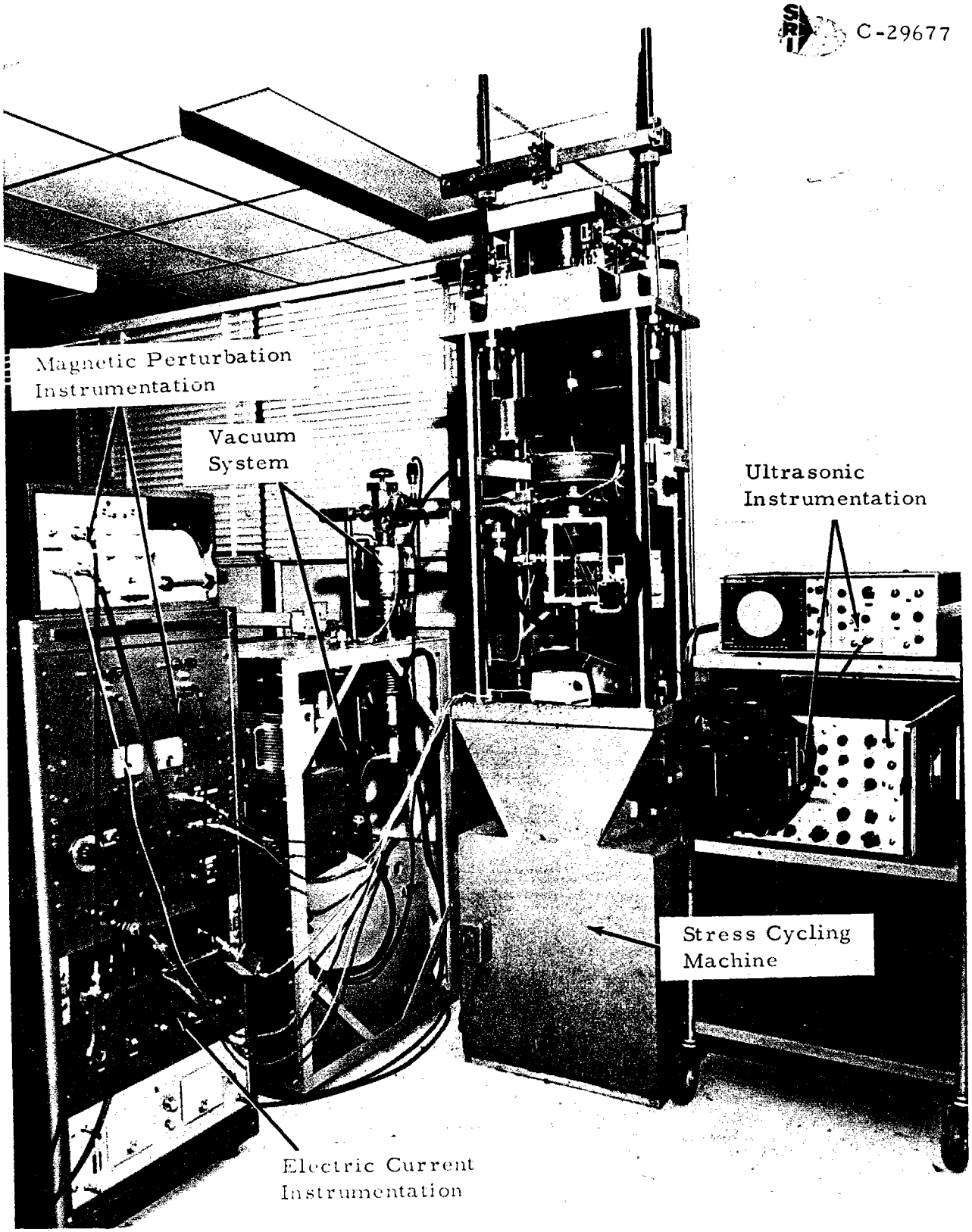

Fig. 3. Overall view of nondestructive fatigue evaluation facility.

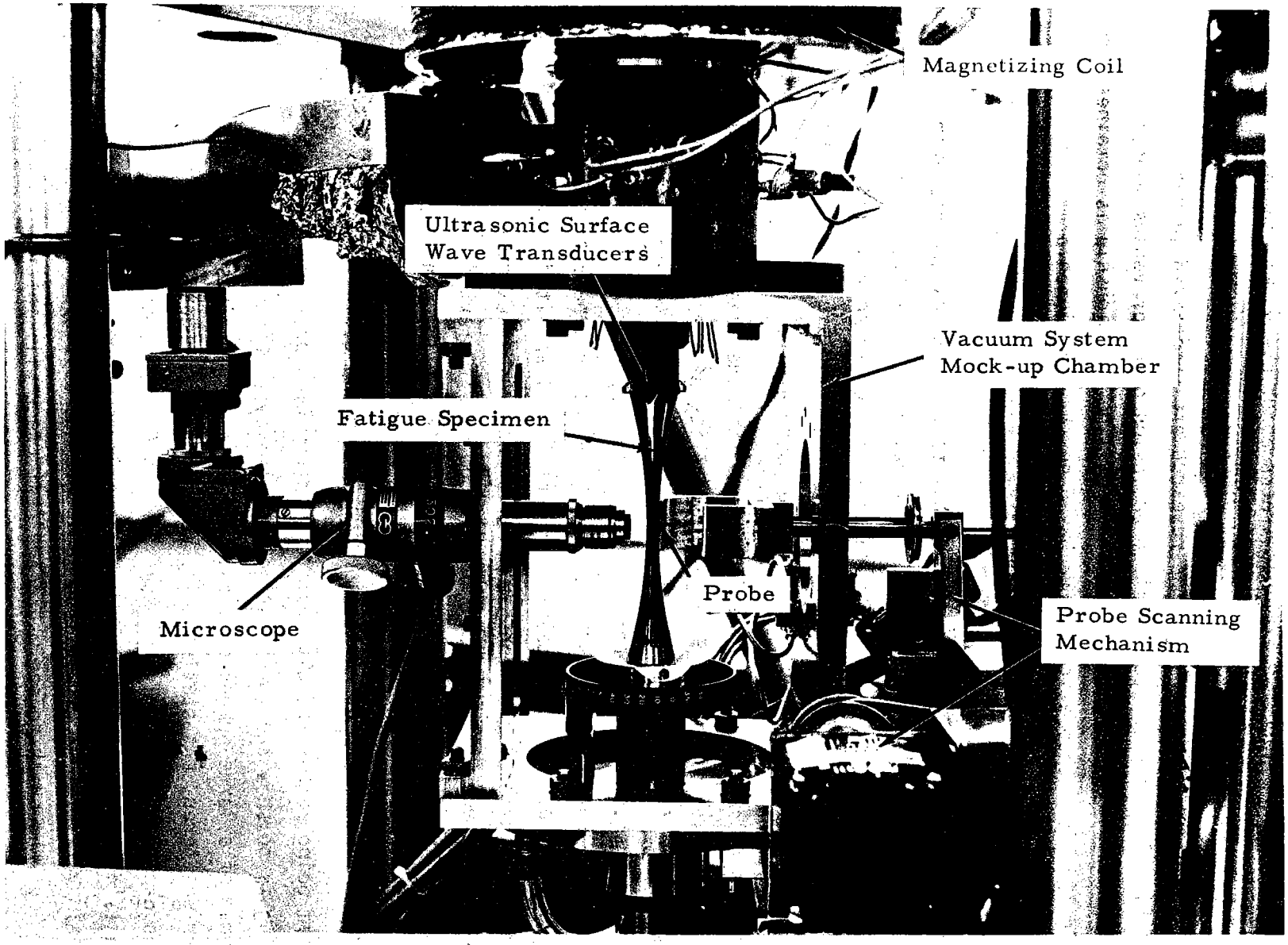

Fig. 4. Close-up view of test specimen and NDE instrumentation mounted in fatigue tester.

With our more recent work, we examined tracks about every two degrees, thereby acquiring quite a large quantity of data.

The quantitative aspects of the research are summarized in the graph of Fig. 5. Here we see a plot of inclusion diameter versus magnetic signal amplitude. As can be seen, a straight line relationship is obtained. The solid line is a theoretical curve based on the relationship

$$S = K d^n$$

where signal amplitude, S, is equal to a constant, K, times the diameter, d, of the flaw to the exponent, n. Theoretically, if an infinite matrix is considered the exponent should be three. So, for these kinds of specimens, and for the flaws that we are finding which are very near the surface, this relationship holds true rather accurately.

Perhaps of more importance is whether or not the size of the inclusion has a quantitative relationship to the criticality of the inclusion. In Fig. 6 such experimental data are plotted. Here we have stress cycles to initiate, or I should say, to both initiate and propagate a crack 0.003 inch long. The horizontal axis is number of cycles to generate such a crack size, and here the vertical axis is the signal amplitude. A fairly well-defined functional relationship is obtained. As an example, here, upper left, is a very large signal and, of course, it started a fatigue crack and propagated to 0.003 inch length at a fairly low number of cycles, about 40,000. The handbook for fatigue life on this material at the stress amplitude that we are using is roughly 100,000 cycles.

I am going rather rapidly over this information because I think the main thing is to show the quantitative relationship. Figure 7 is an S/N diagram of a large number of these specimens. The points seem to be rather scattered, but statistically we find that our data points fit the handbook S/N curve fairly well as shown in Fig. 8. Usually, the specimen is not cycled to fracture. We take it to where a fatigue crack of approximately 0.010 to 0.015 inch in length has developed and then we polish out the crack to see where the next crack will initiate in the

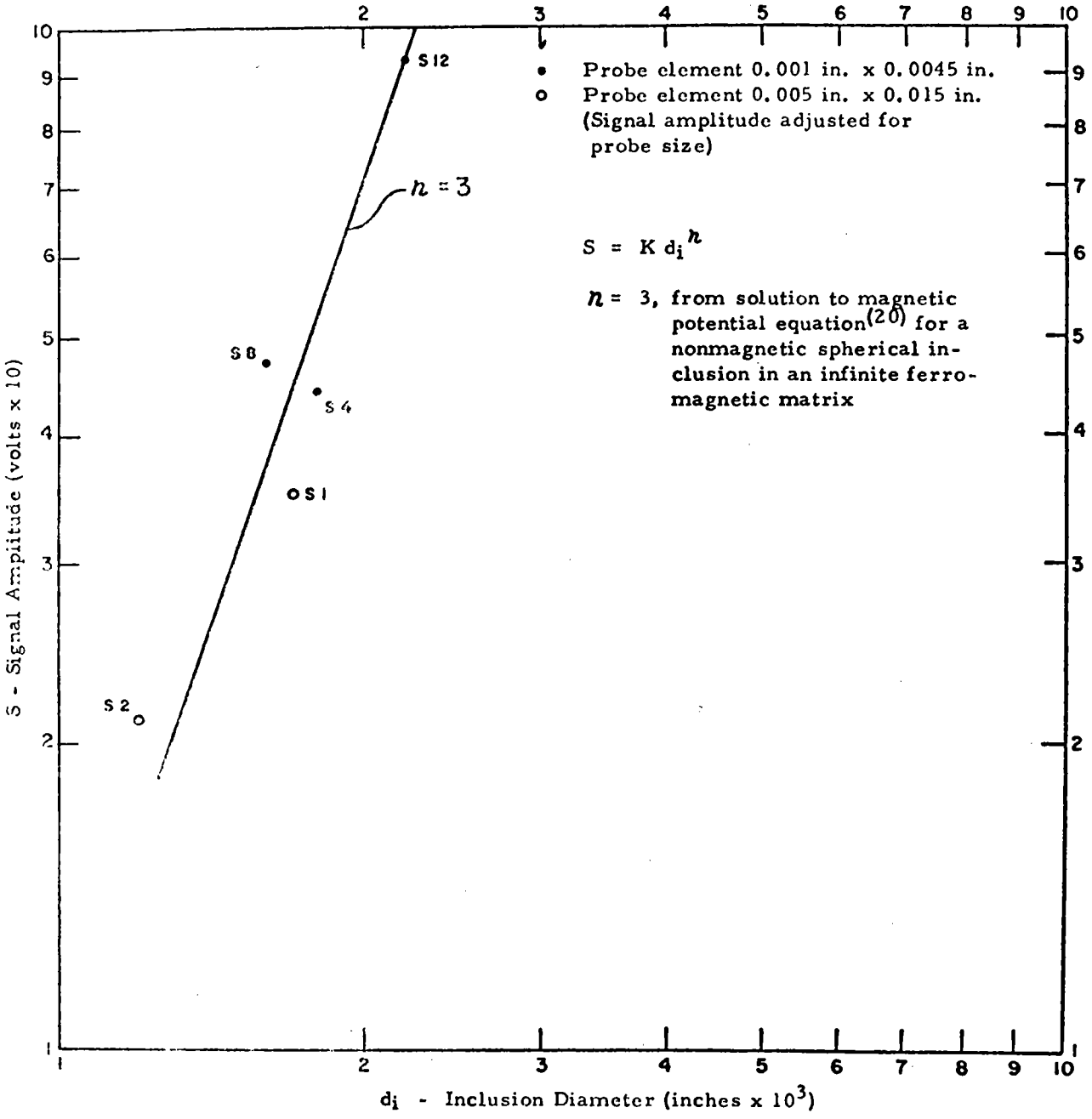

Fig. 5. Functional dependence of magnetic signal amplitude on inclusion size.

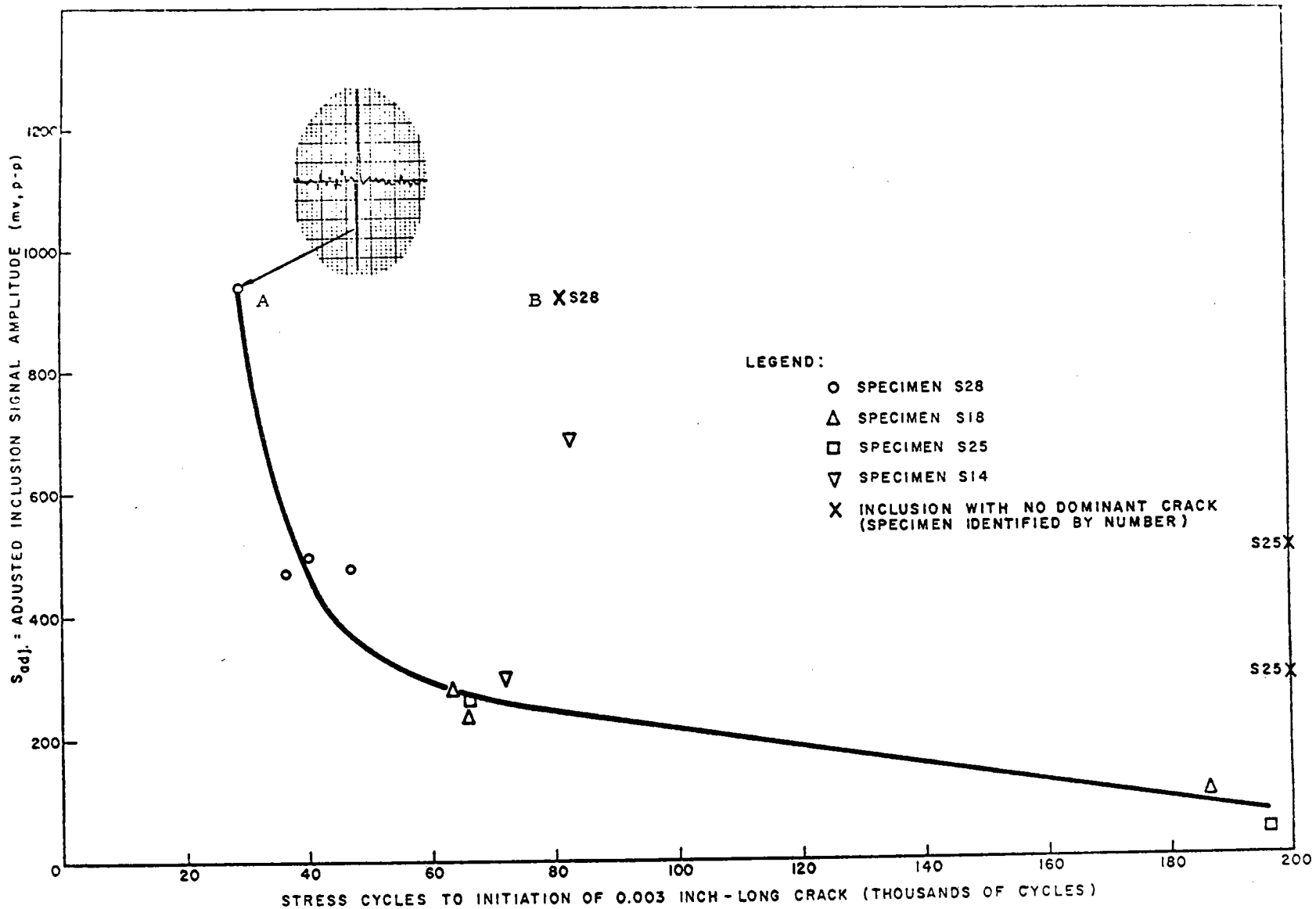

Fig. 6. Precycle inclusion signal amplitude versus stress cycles to initiation of 0.003 inch-long crack.

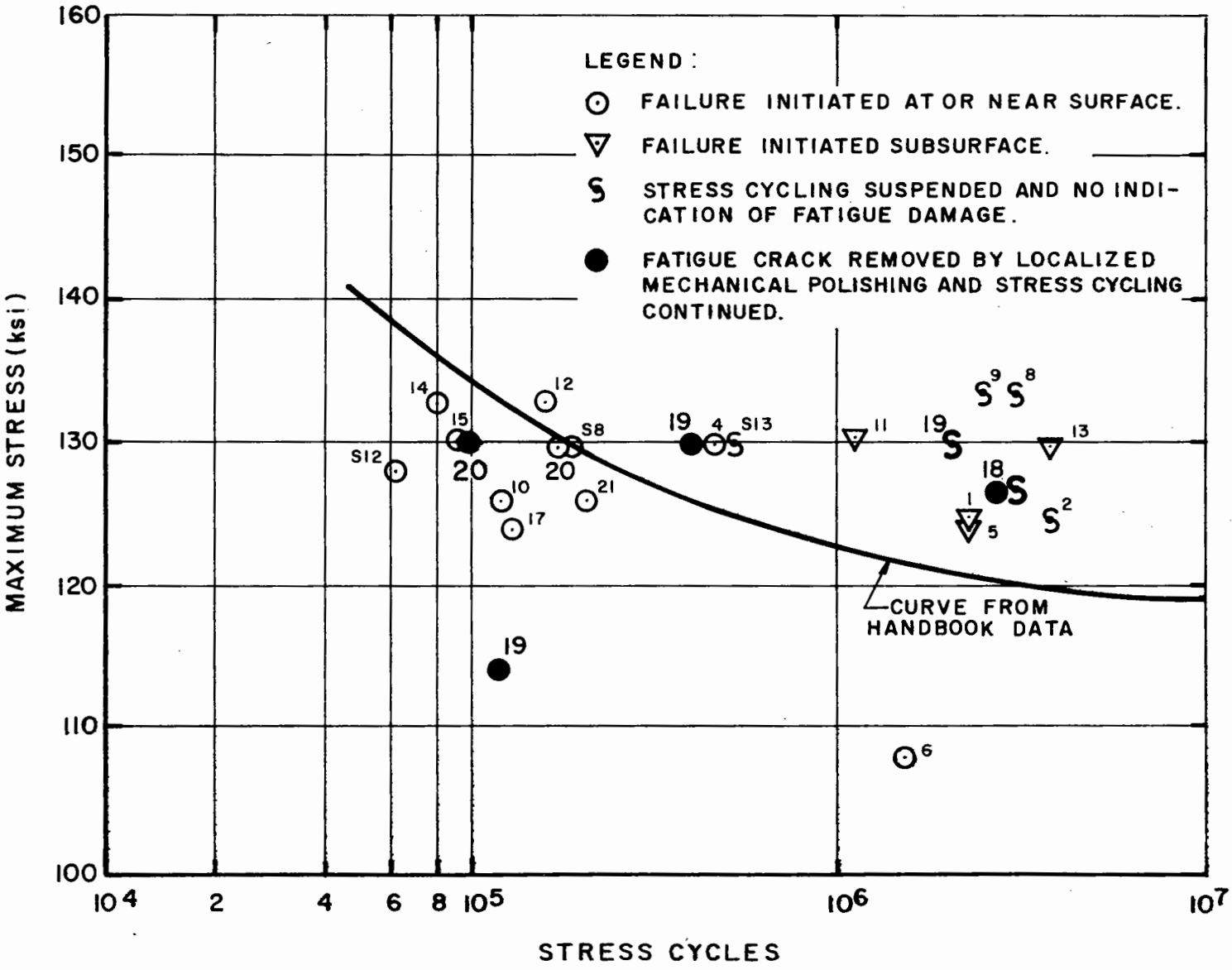

Fig. 7. S-N diagram on specimens.

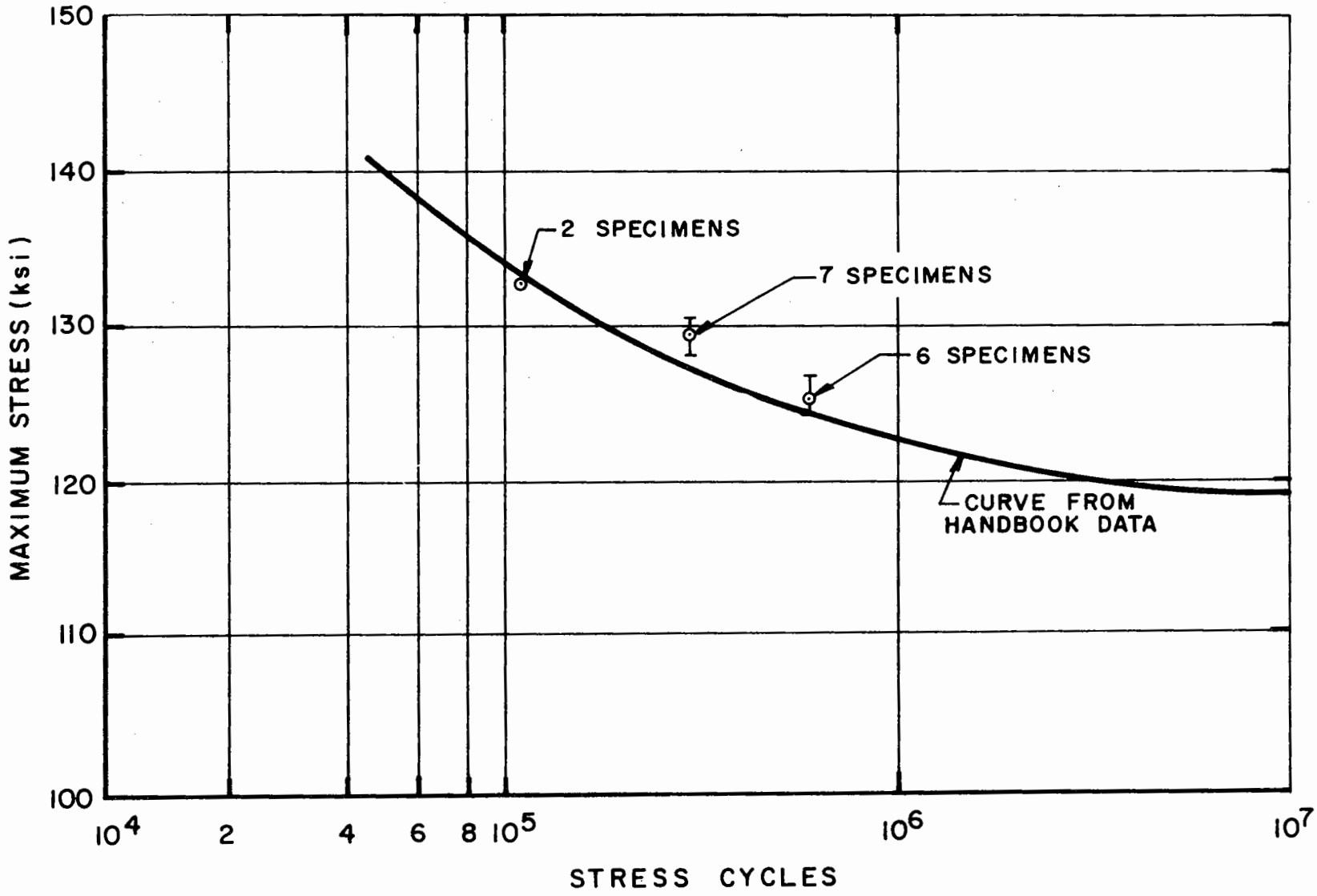

Fig. 8. Statistical comparison with handbook curve.

specimen. The vertical coordinate is the section stress at the inclusion-crack location and the horizontal coordinate includes the actual cycles plus the estimated cycles to fracture (usually 30,000 to 60,000 depending on crack length).

Specimen 19 is a very interesting point in that it is well below the endurance level of the material, and yet a crack did develop. We had not really scanned over this area with our magnetic probe, but we did sense the crack before the specimen went to fracture by means of ultrasonic transducers, bonded to six flats at one end of the specimen; and we were using surface waves at 10 MHz to continuously monitor the specimen during cycling.

The crack is shown in Fig. 9 and, as you see, it is a fairly small crack. It appears to have two different segments; magnification is 150X. After a little of the material was polished from the surface, two separate inclusions were disclosed as shown at the lower left. Also, as can be seen, a separate crack extends from each inclusion. We believe that the fact that the two inclusions were very close together was the reason why this specimen initiated cracks well below the endurance limit.

We removed the inclusions and cracks, continued to cycle the specimen, and the next crack occurred at 377,000 cycles. This second crack that originated in Specimen #19 is shown in Fig. 9B. As you can see, it is a surface inclusion, and at this time apparently only has a crack from one side. We continued to cycle Specimen #19, after removal of the second crack, and ended up over 2×10^6 cycles; cycling was then discontinued.

In Specimen #20, Fig. 7 and Fig. 9C, the crack initiated at 68,100 cycles, and we plotted it at the 10^5 cycle point on the S/N curve, at which it would have fractured. The crack was removed and the specimen subsequently fractured at 180,000 cycles.

Now bear in mind, these specimens are uniaxial tension specimens, no bending loads, so the section stress should be relatively uniform. Nonetheless, cracks selectively originate at the surface and near surface

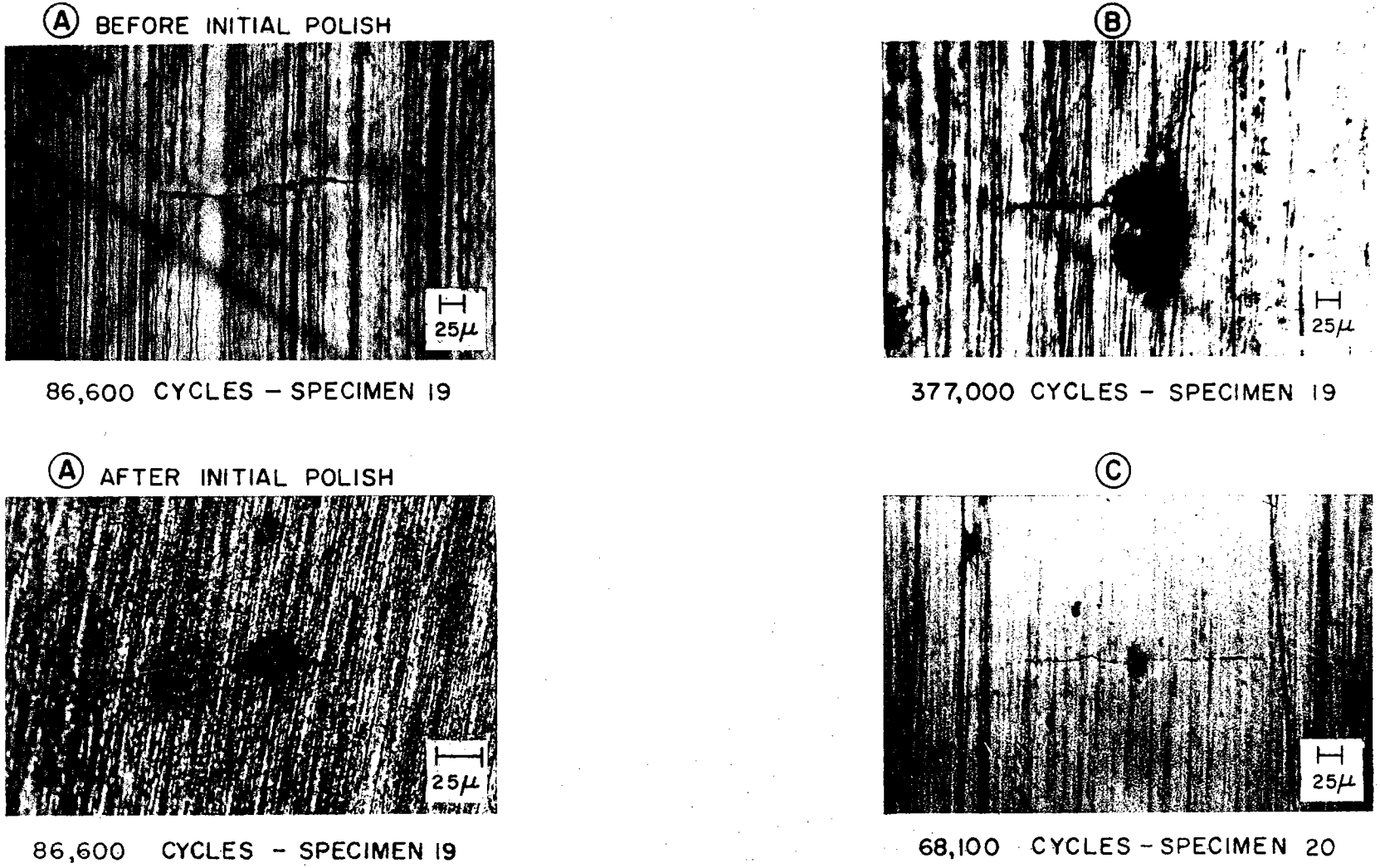

Fig. 9. Photomicrographs of surface fatigue cracks in specimens 19 and 20.

inclusions; fracture is initiated from inclusions deep in the material only at high cycles, $>10^6$. A perspective appraisal of this situation is presented in Fig. 10. This is a composite showing the surface, a very tiny crack, and the source of the crack development is a slightly subsurface inclusion. If we consider only the region over which the section stress varied by only $\pm$ one percent from the maximum stress, a cylinder 0.2 inch long is obtained. If we calculate the volume of that total cylinder and form the ratio of the volume of that cylinder to the volume of the flaw (inclusion), we find that ratio to be one to 19 million, emphasizing the very critical role that these surface and near-surface inclusions play. In other words although the inclusion could have been any place in this total volume, the fact it was near the surface established that it would play a dominant role in crack initiation. If we consider only the surface layer, we get a slightly different ratio. The number reduces to one part in a million, still, such a large ratio that it shows the significance of the near surface flaw as opposed to flaws being located down in the interior. We have seen a few specimens fail with the flaw down in the interior, but generally with a very long fatigue life, in the order of about one to two million cycles.

To emphasize a little bit more dramatically what might take place if on critical specimens we could examine and remove the flaws, both surface and near surface, here is a specimen, Fig. 11, from which thirteen such inclusions were removed. Figure 12 is the bargraph that resulted on that specimen, specimen #15. The specimen has never developed a crack, even after 2.5 million cycles, and no changes have been observed magnetically or ultrasonically. Cycling has been terminated because by the time you get up to this kind of life, it gets very expensive for a small percentage additional life. If we remove this one fairly long-lived specimen #6, and we sum the lives of all these other specimens, they are still less than the life of this one. We do not know how long this specimen would live, but the comment was made by Mr. Darcy this morning that perhaps we could use lower quality materials in some applications. I think these kind of data support that comment, that if you can inspect

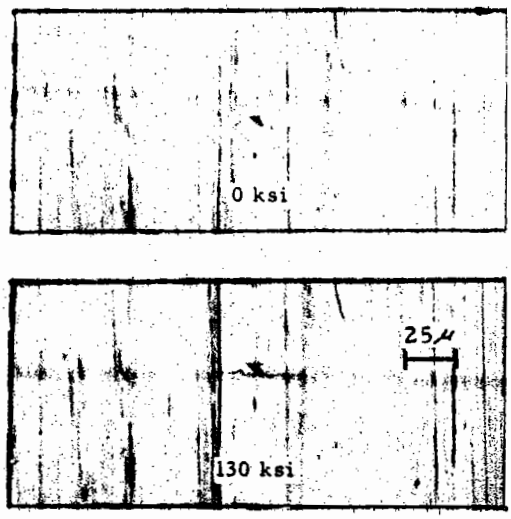

Surface Photomicrographs
at 20,000 Cycles
(For 0- and 130 ksi Static Stress)

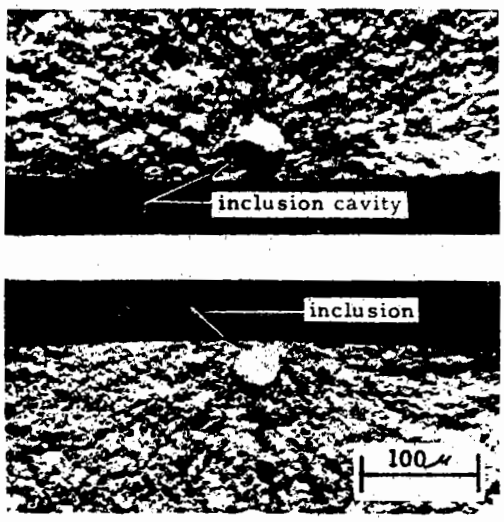

Photomicrograph
of Fracture Surfaces
(Fracture at 62,949 Cycles)

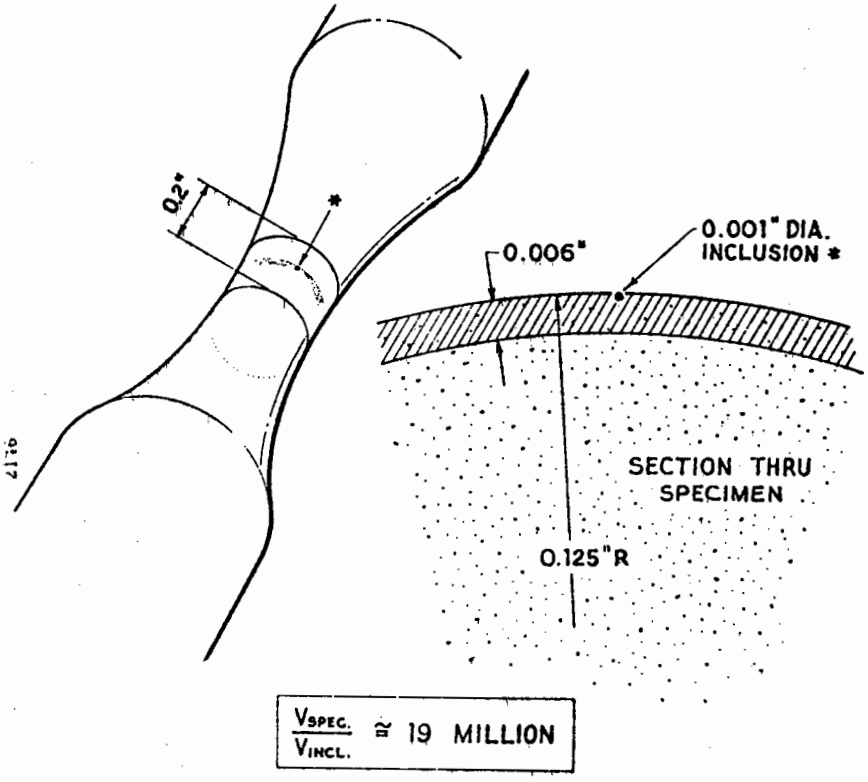

Fig. 10. Fatigue crack initiated at subsurface inclusion and subsequent fracture surfaces.

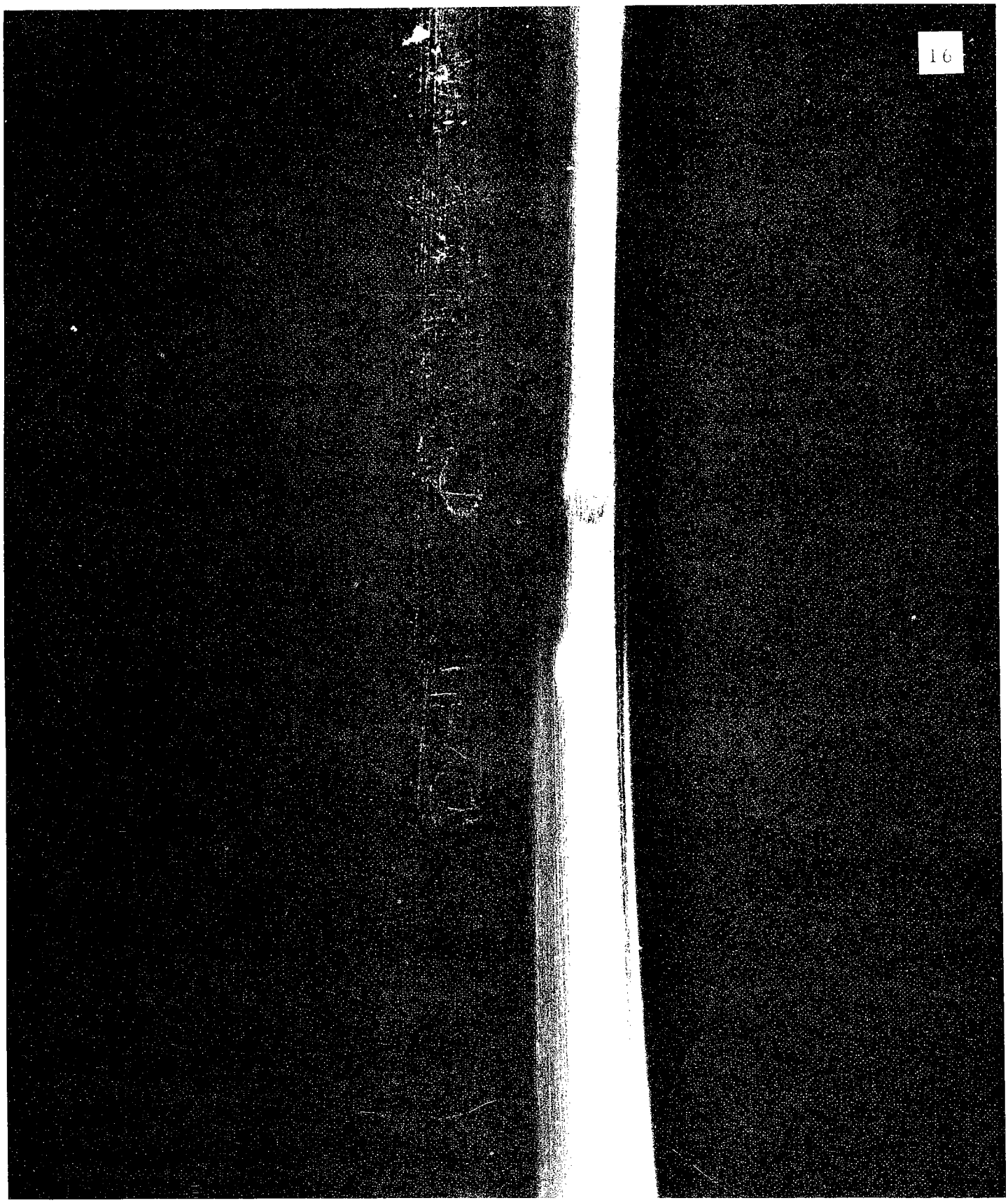

Fig. 11. Specimen S15 with surface inclusions removed

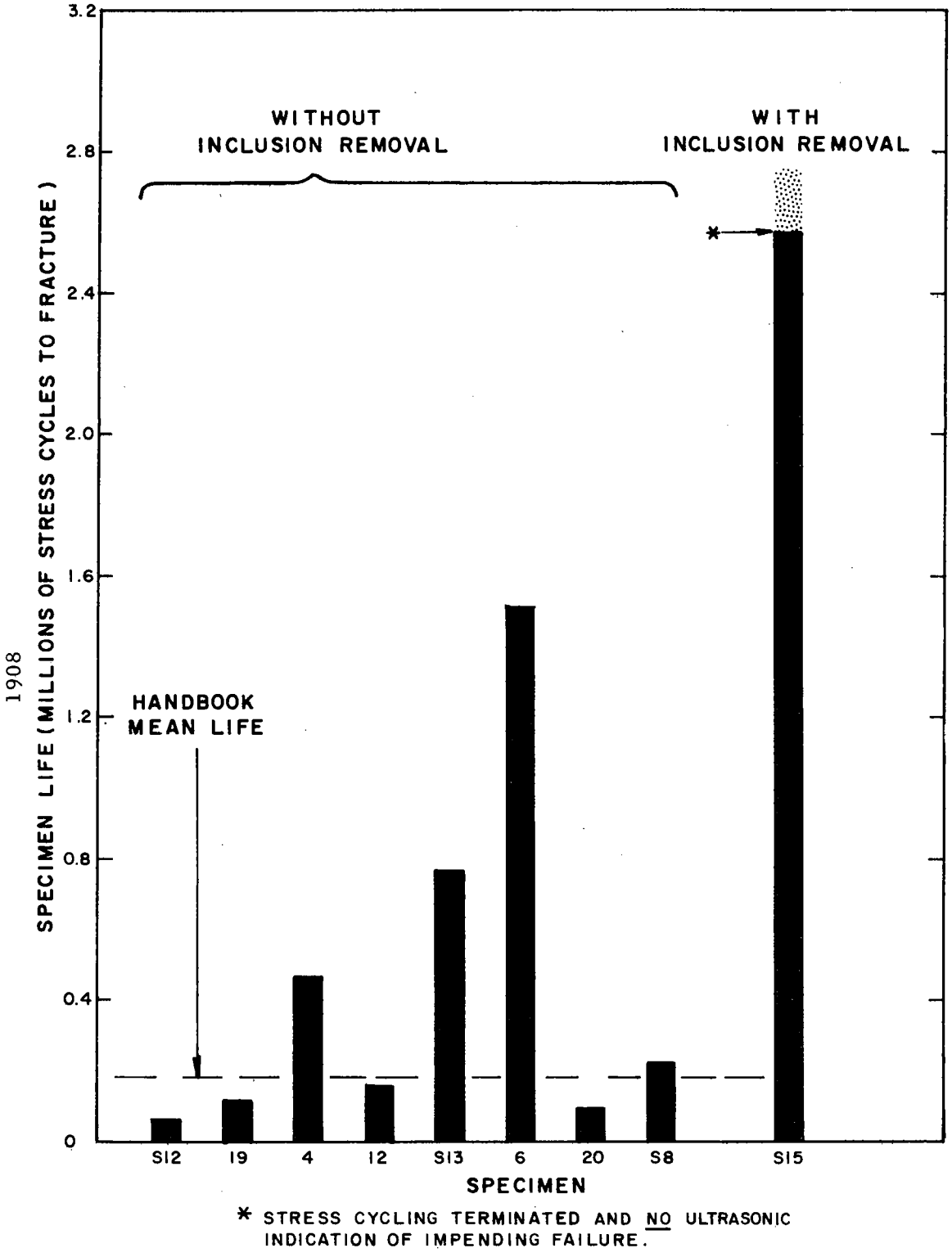

Fig. 12. Bargraph of specimens.

properly, you might be able to use, say, air-melt materials in place of vacuum-melt materials for certain a-plications.

These are rather elegant rod-type specimens, but what happens in the complex kind of loading that you would experience in bearings? We have looked at some ball bearings and I will show you some results.

Figure 13 shows the correlation between a signal and precision metallurgical sectioning disclosing an inclusion. This is one revolution completely around the bearing race, and we are looking at a data track about 0.025-inch wide, so it takes quite a few tracks to look at the whole surface of the bearing. If we expand the signature, it has the general shape shown; from parameter d the approximate depth of the inclusion beneath the surface can be determined independent of the amplitude.

Here is the way we go about correlating our sectioning results. A fine scribe line is made on the bearing surface (we are going to destroy the bearing anyway) and data are rerun (usually, we put two scribe lines on the bearing in an attempt to pinpoint the inclusion region between the two scribe lines; in this instance we missed as can be seen). The distance between the two scribe lines is measured on the race and on the expanded record; the distance from the scribe line signature to the inclusion signature is measured and a proportionate distance on the surface of the bearing race establishes the inclusion location. The 0.005-inch diameter circle marks this location. We can predict the sectioning result on the small inclusions to within about 0.001 inch. Accordingly, sectioning can proceed rather rapidly.

Other examples showing correlation are presented in Figs. 14 and 15. Inclusions can be detected and located with this method, but do these inclusions cause failures in bearings? That is a question that has been raised often, "Do inclusions really cause failures in bearings?"

In Fig. 16 a magnetic inspection record made at zero hours shows an outstanding signature. After the bearing had been run 62.7 hours,

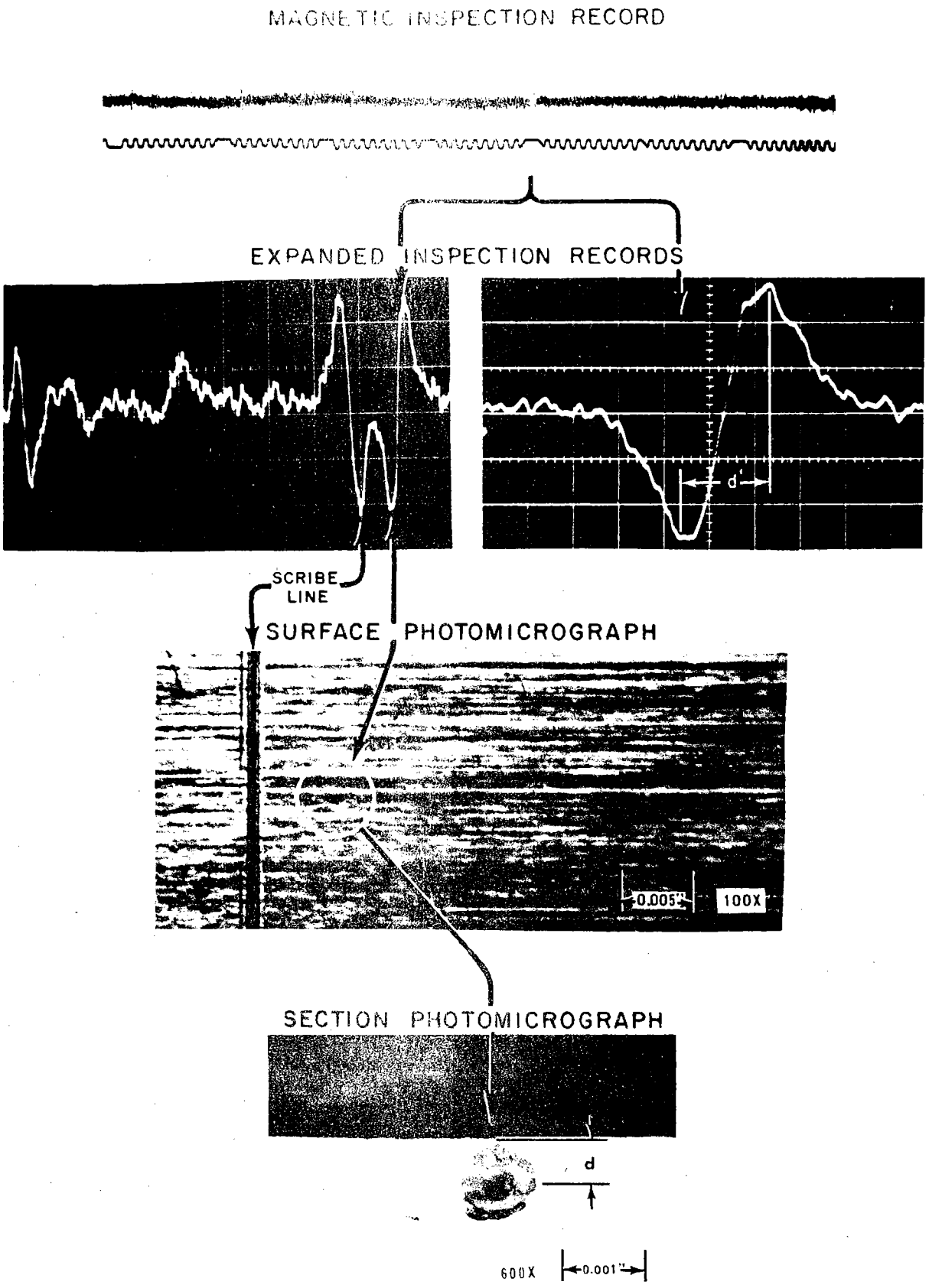

Fig. 13. Detailed method of correlating magnetic perturbation signature with inclusion.

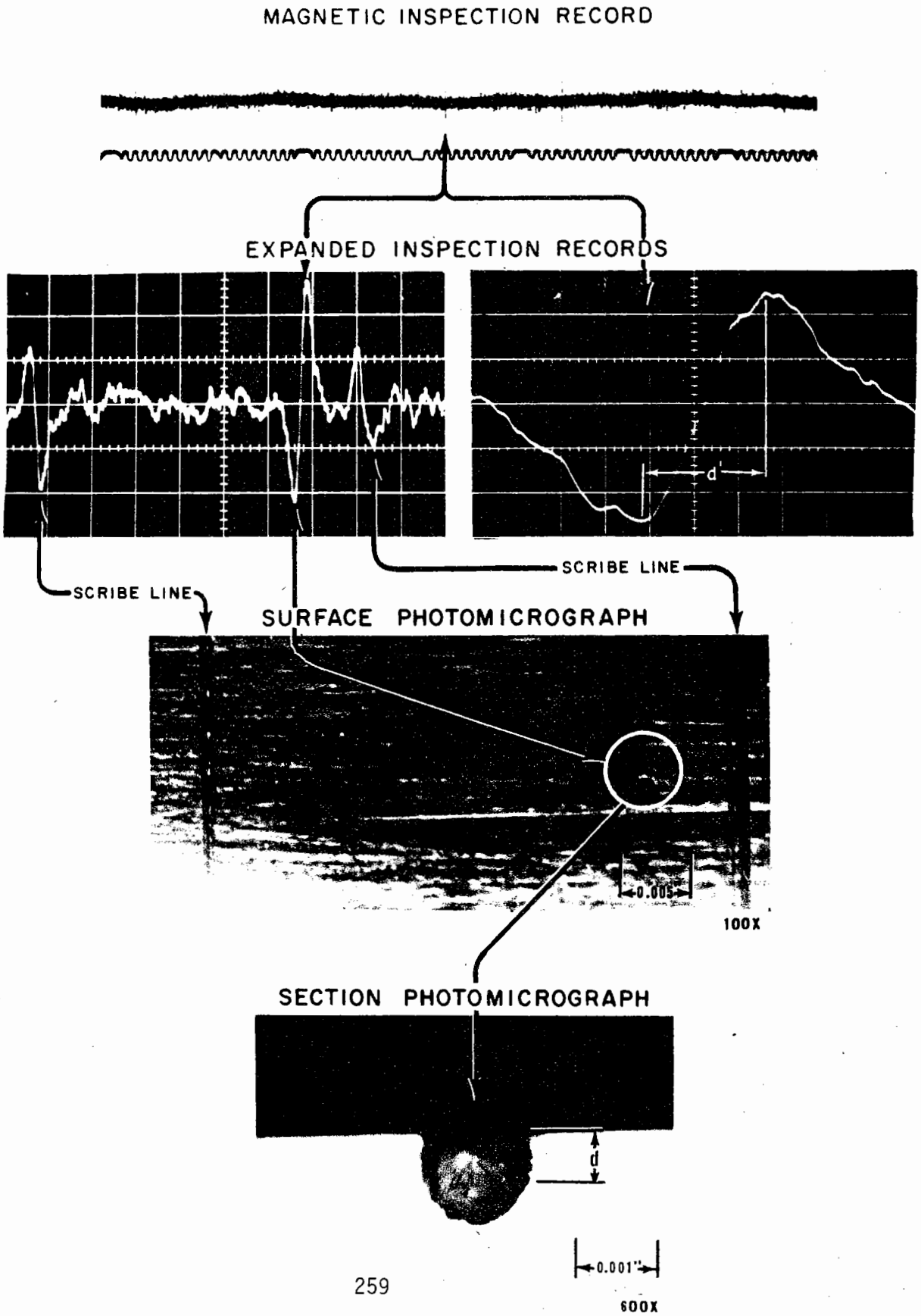

Fig. 14. Correlation of signal and surface inclusion.

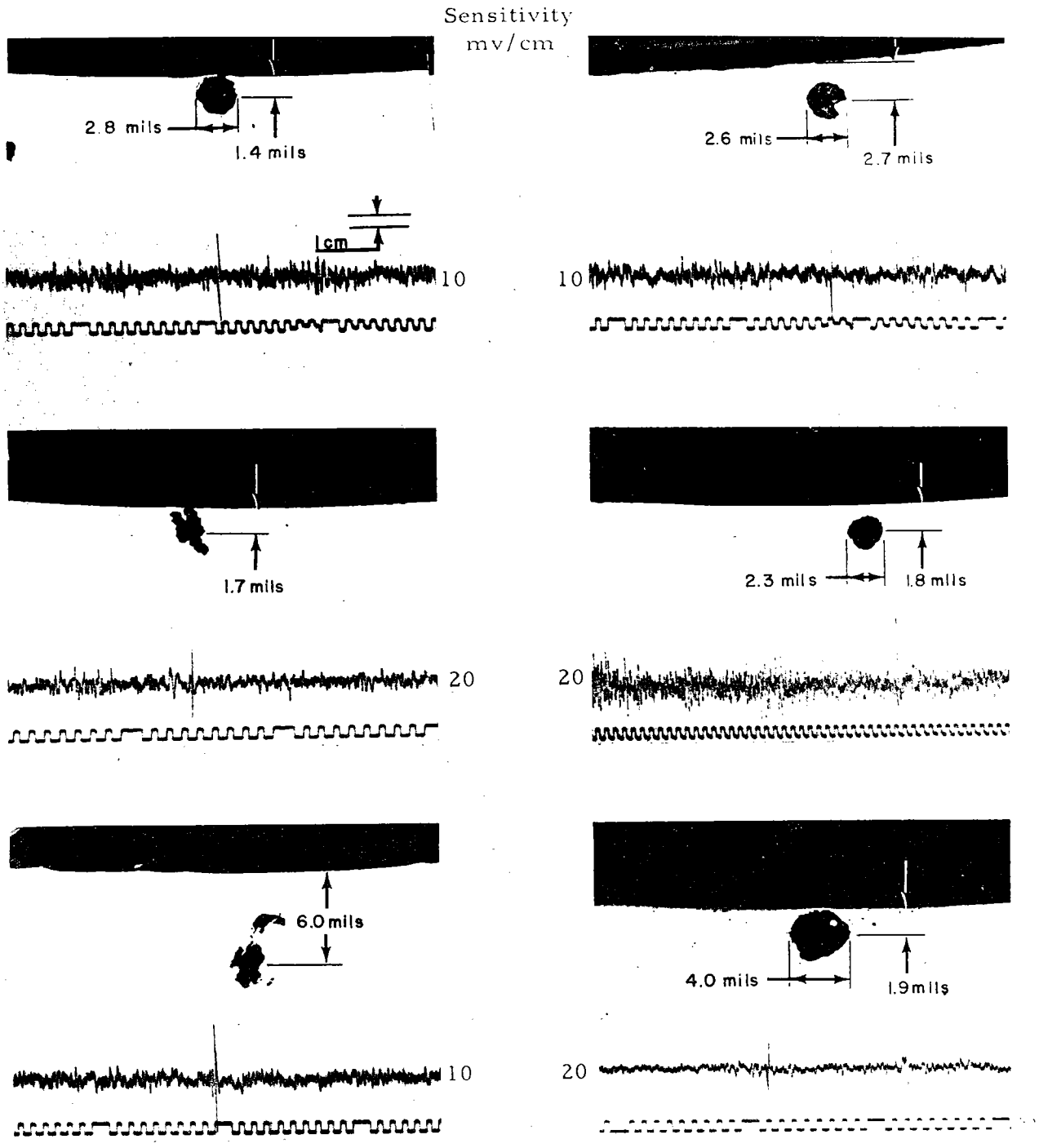

Notes: 1. Sections show ring cross section.
2. All magnifications 100X.

Fig. 15. Correlation of magnetic inspection signals and inclusions in ball bearing inner races.

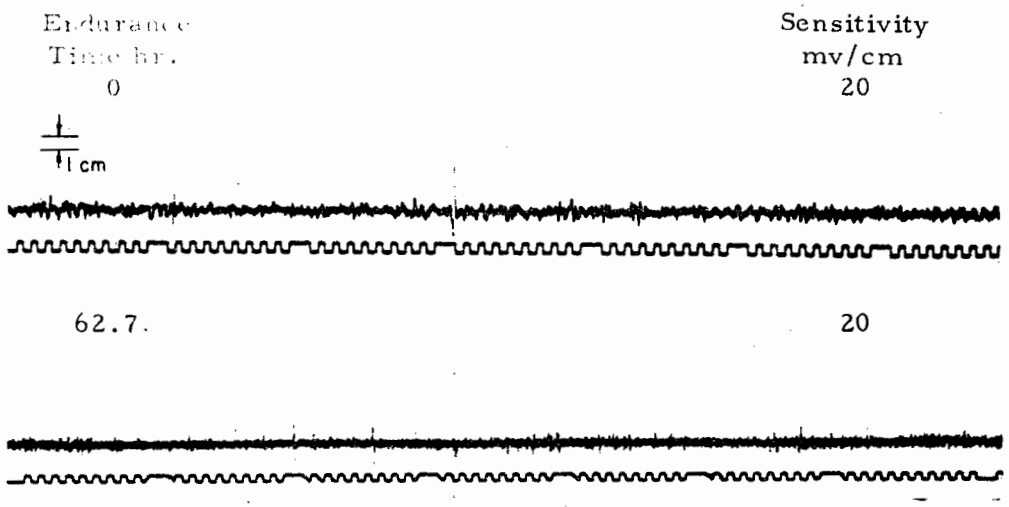

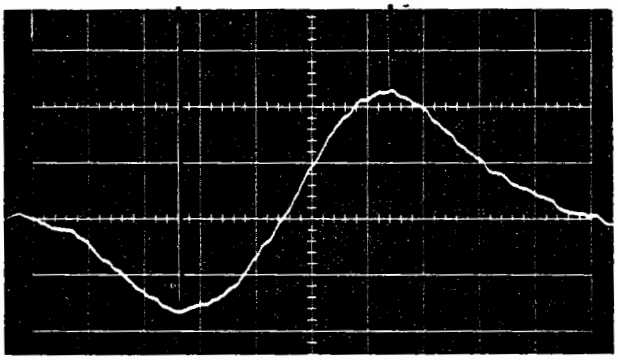

Expanded Trace

Ball Movement

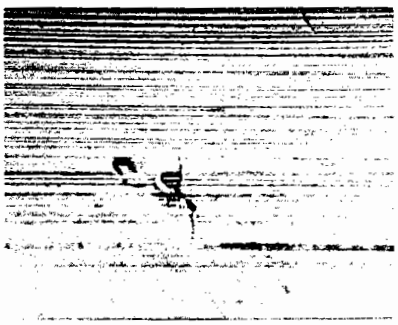

Magnification
90X 100X

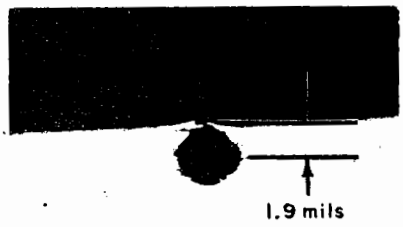

Surface Photo

Sectioning Photo

Fig. 16. Magnetic signature and early stage of spall development.

it is obvious, from the surface photomicrograph that the surface is beginning to crack. The sectioning result shows a very large inclusion and you can see the little lip of the material tilted up. This would have resulted in a spall; I can not predict the number of hours, but it would not have run a hundred hours.

In a program for NASA's Lewis Research Center 103 inner race bearings were inspected. Of these 103 specimens, 23 had inclusion signatures, a few of which were as outstanding as the one shown in Fig. 17. The lower trace markers are to tell us angularly where we are located physically on the bearing race. The outstanding signature is located at 308° in the upper trace obtained before endurance testing. After the bearing had failed at 1,333 hours, the lower record was obtained; the outstanding excursion corresponds with the spall region. Physically, the leading edge of the spall correlated precisely with where we had our indication at 308°. Data clearly illustrating the correlation between an inclusion signature and failure initiation on Specimen No. 24 are presented in Fig. 18. The photograph of the bearing surface obtained prior to endurance testing in the region containing the initiation point of the subsequent spall shows a high-quality bearing surface with no observable flaws. Again analysis of the angular location and extent of the spall in conjunction with the magnetic records indicates that the inclusion signature at 12° was located in the extreme leading edge of the spall. Examination of the leading edge at high magnification using bright field illumination (lower left illustration) showed no evidence of the initiating source. However, polarized light illumination of this region disclosed a small inclusion approximately 2.7×10^{-3} inches in diameter, and this inclusion was the initiating source for the spall development. The double exposure with the bright field and polarized light clearly shows the location of this inclusion relative to the leading edge of the spall.

In Fig. 19 Weibull plots are presented from a NASA report generated around some other data, but still based on these same bearings.

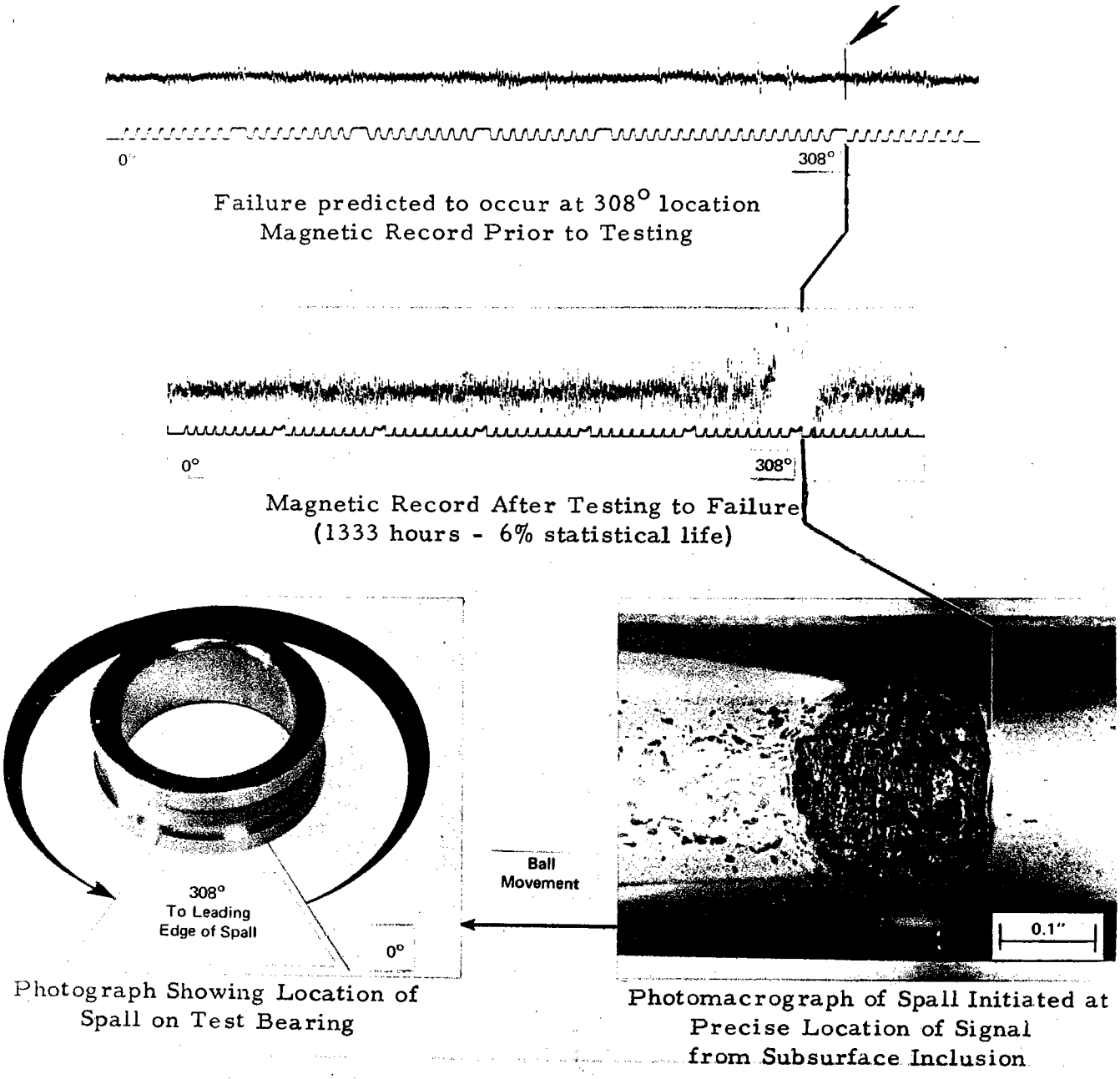

Fig. 17. Failure initiation at inclusion signature on specimen #130.

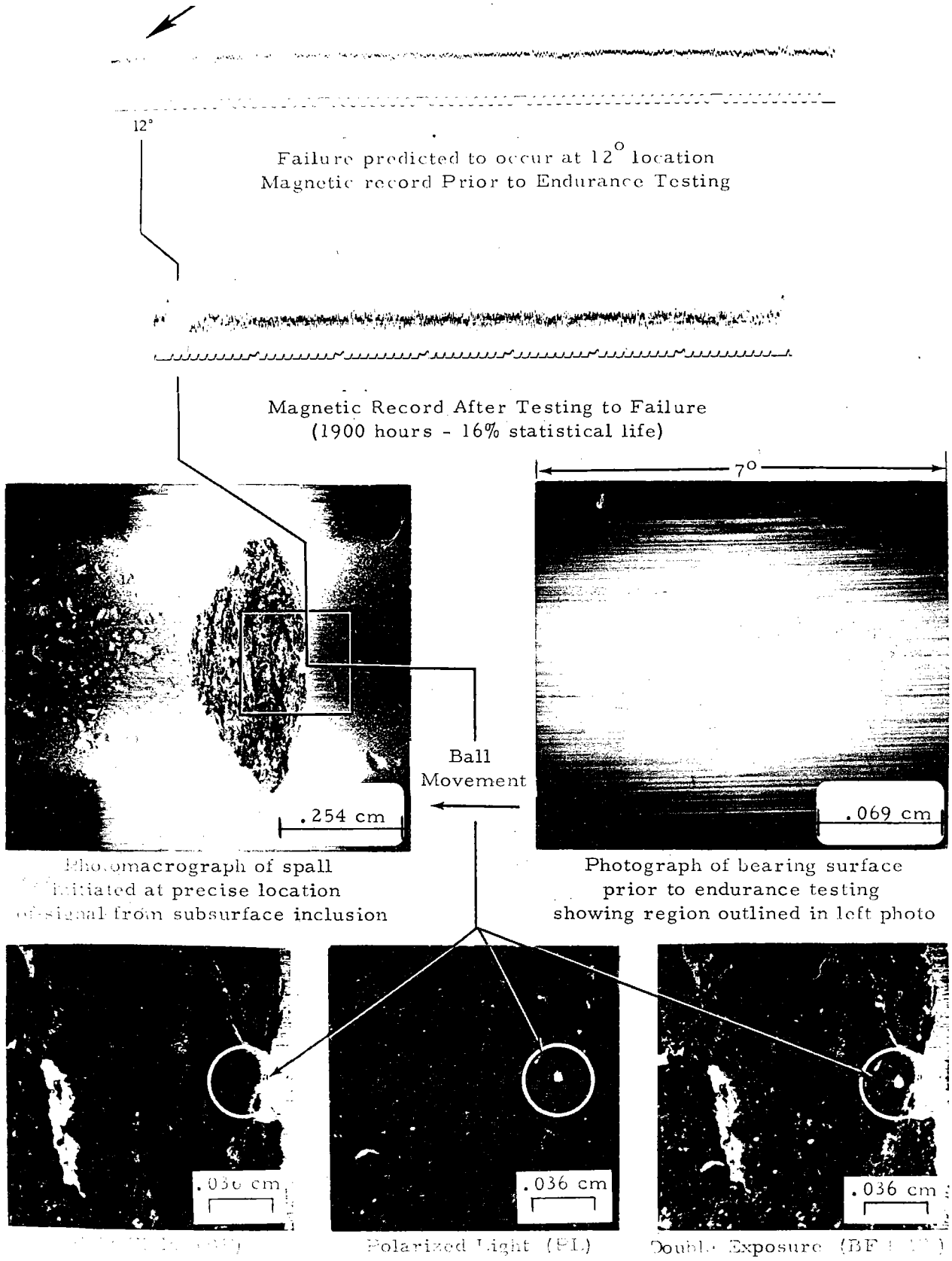

Fig. 18. Failure initiation at subsurface inclusion on specimen #24.

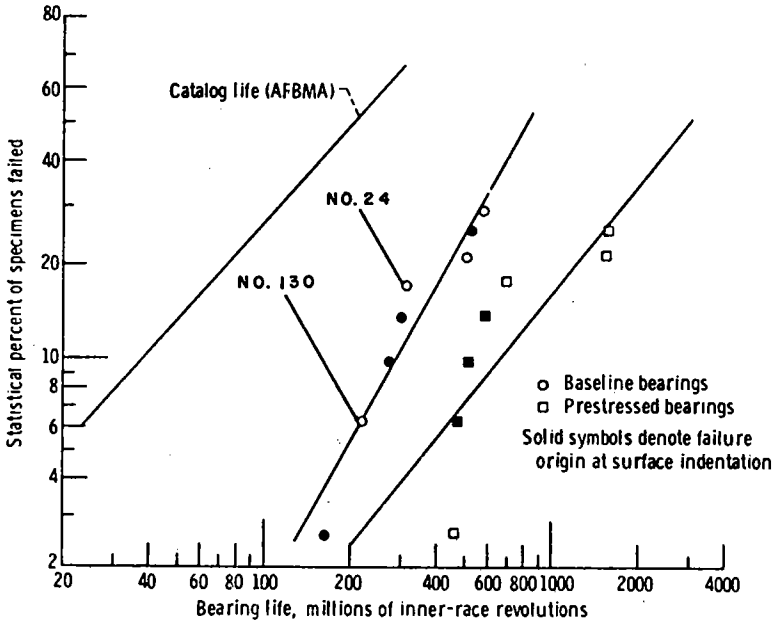

Fig. 19. Results of fatigue tests with 207-size ball bearings tested at a radial load of 5860 newtons (1320 lb) and a shaft speed of 2750 rpm with a super-refined naphthenic mineral oil.

Only 54 of the 103 bearings were tested, and they were divided into two groups of 27 each. One group was subjected to a limited-time over-stress run prior to endurance testing; the other group was used to establish a baseline. These bearings were all better than the catalog-rated average life as seen in Fig. 19.

The catalog life data, I have been told, were generated some years ago and are not really of much use anymore since most bearings greatly exceed this life today. First we consider the Weibull plot on the baseline bearings. The only two failures that correlated with the magnetic perturbation signatures were specimens #130 and #24. The people at NASA Lewis were quite disappointed. They expected, I would presume, that all failures would be located at inclusion signatures. However, this was not the case and the basis of why this did not happen will be presented later.

On the Weibull plots, the solid symbols denote failure originating at a surface indentation. These are probably caused by debris in the oil or from some source; particles become interposed between the balls and the race, and what is known as an indentation is produced when the ball rolls over such particles. Indentations are very detrimental and cause many bearings to fail. If we eliminate from the baseline plot specimens which failed from indentations, only four points are left to define the Weibull plot and, accordingly, the statistical confidence is not high. Even so, with the statistics as they are, the important factor observed is that the first two failures obtained were specimens #130 and #24 at 6 percent life and 16 percent. These were, in fact, the only early failures in the whole group of bearings, and the early failures are the ones you would like to eliminate.

We should now clarify the situation concerning why some inclusions caused failures while others did not. Factors which should be considered are: inclusion size, type, location in relation to the contact surfaces, location with respect to the center of the load zone, residual stresses, etc. Table I. presents quantitative information on the ball bearings containing inclusion signatures which were endurance tested. The first

TABLE I

QUANTITATIVE NDE RESULTS ON BALL BEARINGS

Signal Amplitude	Ring No.	Axial Location	Hours	Sectioning Size cm x 10^{-3} (in x 10^{-3})
67	24	7.7°	1,902	6.8(2.70)F
60	48	18.2	1,826	-
58	130	2.5	1,333	- F
53	6	347.0	P 10,000	2.54(1.00)C
49	85	347	4,000	7.0 (2.75)
47	120	357.5	P 10,000	2.3 (0.90)
39	3	3.5	4,000	3.8 (1.50)C
38	69	23.5	P 10,000	3.05 (1.20)
36	82	357.5	P 10,000	-
35	148	18.2	P 9,655	-
30	25	352.2	P 9,940	2.8 (1.10)
29	110	347	3.635	-
25	129	2.5	4,000	-
25	74	2.5	3,126	2.5 x 11.5 x 0.25 (1.0 x 4.5 x 0.1)
22	23	7.7	P 10,000	3.8 x 6.3 x 0.5 (1.5 x 2.5 x 0.2)
22	89	357.5	P 10,000	-
20	96	18.2	-	-
20	7	2.5	3,077	-

Notes:

a. 103 bearing inspected
b. 23 inclusion signatures
c. 54 bearings endurance tested (20 with inclusion signatures)

F = failed at inclusion
C = cracking at inclusion
P = prestressed

column tabulates the signal amplitude in the sequence of largest amplitude at the top and smallest amplitude at the bottom. The axial location specifies the location across the ring groove at which the signature was obtained; as will be shown in a subsequent figure, the extent of the plastic zone determined during etching of metallurgical sections was contained within the angular limits $\pm$ 10.5°. Accordingly, this angular location provides a basis for appraising the severity of the inclusion in relation to the running stresses encountered at that location. A perspective appraisal of these data are depicted in the schematic illustration of Fig. 20. This illustration shows the locations, relative size, depth of the inclusions (that were confirmed by metallurgical sectioning or estimated from the magnetic signatures) relative to the race surface and the highly stressed zone of resolved shearing stresses. The specimen number, endurance test time, and amplitude of magnetic signature are indicated for each specimen. From this diagram it should be obvious that some of the inclusions have very low potential for initiating failure because of the low running stresses encountered in the regions where they are located. For example, 69, 48, 148, and 85. Note that Specimen 130, which was the earliest failure at an inclusion, is located near the center of the load track and slightly above the plastic zone. The inclusion in Specimen 24, which was the only other inclusion initiated spall, is approximately midway between the surface and the upper edge of the plastic zone; although this specimen had a 67 millivolt signature indicating that the inclusion was somewhat larger than for the 58 millivolt signature of Specimen 130, the life of this specimen was 43 percent greater than for 130. The decreased stresses at this axial location may have accounted for the increased life. Several other inclusions, for example in specimens 120, 129, 82, 7, and 3, were located very near the center of the load track and yet did not initiate failure. Specimen 3 has small cracks at the inclusion after 4,000 hours. It is suggested that residual compressive stresses in the near surface layer of these races may have minimized crack initiation at these inclusions. Residual stress measurements

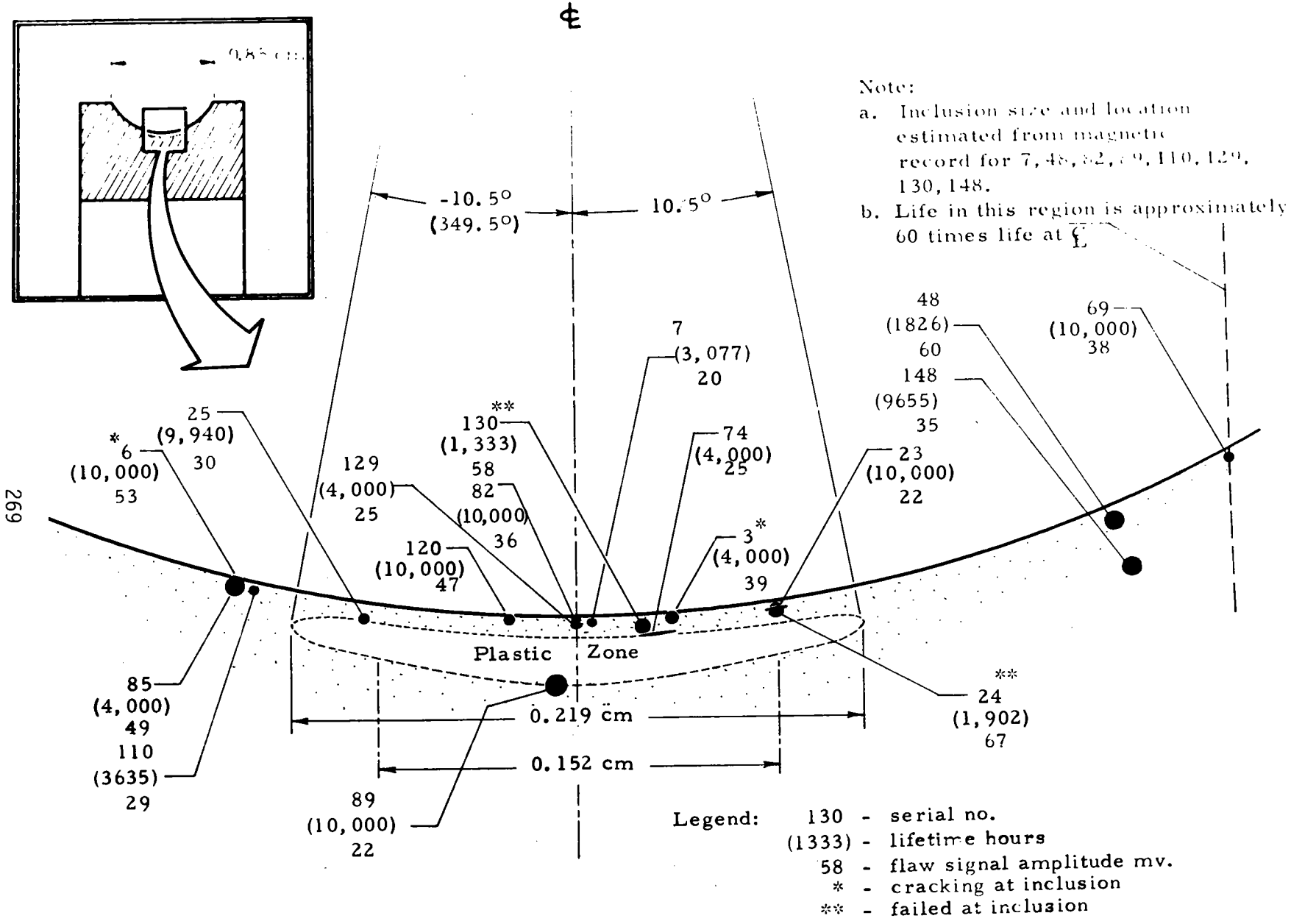

Fig. 20. Schematic showing inclusion locations and subsurface plastic zone.

made, on several of the bearings endurance tested, by using X-ray diffraction and progressive etching showed the surface to be in residual compression. A minimum compressive stress existed at a point approximately 1.5 to 2.0 x 10^{-3} inches beneath the surface, thereafter becoming more compressive. It was also recently reported that tension stresses are developed at the upper edge of the plastic zone with extended endurance testing. Accordingly, it is suggested that those inclusions that are near the upper edge of the plastic zone could tend to initiate cracks sooner than those in the compressive region near the surface of the bearing. Two of the specimens contained planar inclusions surrounded by sulfides and, accordingly, should not be severe stress risers.

While it should be recognized that a strong statistical base for assessing the effectiveness of the magnetic perturbation method for minimizing bearing failures has not been provided by the available information, the results reported are significant. Despite this lack of a statistical base, it is important to emphasize that two "early failures" could have been eliminated by rejecting only those specimens with magnetic perturbation signatures greater than 55 millivolts. Of the 103 specimens inspected, only three, 130, 24, and 48, are in this category. Nos. 130 and 24 failed respectively at 6 percent and 16 percent statistical life. Not only were these inclusions large but they were located in a region of high stress, i.e., near the center of the ball track as shown in Fig. 20. Also, these inclusions were 0.0020 inch and 0.0014 inch deep, respectively, which is in the region of minimum residual compressive stress measured on these bearings. The inclusion in Specimen 48 was in a region where the running stresses were relatively low and accordingly, should not have been anticipated to be a failure source. Metallurgical sectioning disclosed cracking at the inclusion in Specimen 3 after 4,000 hours endurance running. To eliminate this specimen, which may have failed with additional endurance testing, would require setting the rejection limit at approximately 40 millivolts. Only nine bearings (3, 6, 24, 48, 69, 85, 120, 130 and 148) from the total group of 103 are in this category; two failed

(24 and 130), two have cracking at the inclusion (3, 6), four are outside the region of high stress (48, 69, 85, and 148), and one was prestressed (120).

In summary, it is suggested that the magnetic perturbation method which has shown excellent potential for predicting cycles to develop inclusion nucleated cracking under simple conditions of stressing, namely uniaxial tension, offers significant potential for developing methodology to predict bearing life.

Acknowlegements

A number of people at Southwest Research Institute have made valuable contributions to the programs which have been the subject of this paper. Noteably, F. N. Kusenberger, W. Lyle Donaldson, R. D. Williams, J. Lankford, Jr., B. F. Stevens, and J. H. Tolle. Appreciation is also expressed to Dr. J. Pomerantz of the Air Force Office of Scientific Research for his interest and support of our fatigue research. The interesting technical discussions, suggestions, and support of S. Goldberg, Naval Air Systems Command and R. J. Parker, NASA-Lewis Research Center, are also gratefully acknowledged.